Astronomy Letters, Vol. 33, No. 7, 2007, pp. 437-454. Translated from Pis'ma v Astronomicheskii Zhurnal, Vol. 33, No. 7, 2007, pp. 492-512.

High Mass X-ray Binaries and Recent Star Formation History of the Small Magellanic Cloud

P. E. Shtykovskiy[1,2*], **M. R. Gilfanov**[2,1]

[1] *Space Research Institute, Profsoyuznaya str. 84/32, Moscow 117997, Russia*
[2] *MPI for Astrophysik, Karl-Schwarzschild str. 1, Garching, 85741, Germany*

We study the relation between high-mass X-ray binary (HMXB) population and recent star formation history (SFH) for the Small Magellanic Cloud (SMC). Using archival optical SMC observations, we have approximated the color-magnitude diagrams of the stellar population by model stellar populations and, in this way, reconstructed the spatially resolved SFH of the galaxy over the past 100 Myr.We analyze the errors and stability of this method for determining the recent SFH and show that uncertainties in the models of massive stars at late evolutionary stages are the main factor that limits its accuracy. By combining the SFH with the spatial distribution of HMXBs obtained from XMM-Newton observations, we have derived the dependence of the HMXB number on the time elapsed since the star formation event. The number of young systems with ages 10 Myr is shown to be smaller than the prediction based on the type-II supernova rate. The HMXB number reaches its maximum $\sim$20–50 Myr after the star formation event. This may be attributable, at least partly, to a low luminosity threshold in the population of X-ray sources studied, Lmin$\sim 10^{34}$ erg/s. Be/X systems make a dominant contribution to this population, while the contribution from HMXBs with black holes is relatively small.

Key words: high mass X-ray binaries, Small Magellanic Cloud, star formation.

* E-mail: pavel@hea.iki.rssi.ru

INTRODUCTION

High-mass X-ray binaries (HMXBs) are close binary systems in which the compact object (a black hole or a neutron star) accretes matter from an early-type massive star. Because of the short lifetime of the donor star, they are closely related to recent star formation and, in the simplest picture, their number should be roughly proportional to the star formation rate of the host galaxy. Indeed, Chandra observations of nearby galaxies suggest that, to the first approximation, the HMXB luminosity function follows a universal power law whose normalization is proportional to the star formation rate (SFR) of the host galaxy (Grimm et al. 2003).

On the other hand, obvious considerations based on the present view of the evolution of binary systems suggest that the relation between HMXB population and star formation should be more complex than a linear one. There is also experimental evidence for this. For example, previously (Shtykovskiy and Gilfanov 2005a), we showed that the linear relation between the number of HMXBs and the SFR cannot explain their spatial distribution over the Large Magellanic Cloud (LMC), because their number does not correlate with the H_α line intensity, a well-known SFR indicator. The largest number of HMXBs is observed in the region of moderate star formation LMC 4, while they are virtually absent in the most active star-forming region in the LMC, 30 Dor. Previously (Shtykovskiy and Gilfanov 2005a), we suggested that this discrepancy could arise from the dependence of the HMXB number on the time elapsed since the star formation event. Indeed, the age of the stellar population in 30 Dor is $\approx 1-2$ Myr, which is not enough for the formation of compact objects even from the most massive stars and, accordingly, for the appearance of accreting X-ray sources. At the same time, the characteristic age of the stellar population in LMC 4, $\approx 10-30$ Myr, is favorable for the formation of an abundant HMXB population. Thus, on the spatial scales corresponding to individual star clusters, the linear relation between the HMXB number and the instantaneous SFR does not hold and the recent star formation history (SFH) on time scales of the order of the lifetime of the HMXB population, i.e., $\sim 2-100$ Myr, should be taken into account. Obviously, the number of active HMXBs at a certain time is determined by the total contribution from systems of different ages according to the dependences of the star formation history SFR(t) and a certain function $\eta_{HMXB}(t)$ describing the dependence of the HMXB number on the time elapsed since the star formation event. The universal relation $N_{HMXB} = A\times$SFR on the scales of galaxies results from the spatial averaging of $\eta_{HMXB}(t)$ over star-forming regions of different ages.

The Small Magellanic Cloud (SMC) is an ideal laboratory that allows these and other aspects of HMXB formation and evolution to be studied. Indeed, owing to its appreciable SFR and small distance (60 kpc), there are dozens of known HMXBs in it. On the other hand, the SMC proximity makes it possible to study in detail its stellar population and, in particular, to reconstruct its SFH. Another peculiarity of the SMC, namely, its low metallicity, makes it potentially possible to study the effect of the heavy-element abundance on the properties of the HMXB population. In this paper, we use XMM-Newton observations of the SMC (Shtykovskiy and Gilfanov 2005b) and archival optical observations (Zaritsky

et al. 2002) to analyze the relation between the number of HMXBs and the recent SFH of the galaxy. Our goal is to derive the dependence of the HMXB number on the time elapsed since the star formation event.

1. EVOLUTION OF THE HMXB POPULATION AFTER THE STAR FORMATION EVENT

To describe the evolution of the HMXB population, let us introduce a function $\eta_{HMXB}(t)$ that describes the dependence of the number of observed HMXBs with luminosities above a given value on the time t elapsed since the star formation event normalized to the mass of the formed massive stars:

$$\eta_{HMXB}(t) = \frac{N_{HMXB}(t)}{M(> 8M_{\odot})} \tag{1}$$

where M(>8 $M_{\odot}$) is the mass of the stars more massive than 8 $M_{\odot}$ formed in the star formation event and $N_{HMXB}(t)$ is the number of HMXBs with luminosities exceeding a certain threshold. The luminosity of 10^{34} erg/s that corresponds to the sensitivity achieved by XMM-Newton in the SMC observations is taken as the latter.

Obviously, the function $\eta_{HMXB}(t)$ is non-zero only in a limited time interval. Indeed, the first X-ray binaries appear only after the formation of the first black holes and/or neutron stars. The lifetimes of the stars that explode as type II supernovae (SNe II) to produce a compact object lie in the interval from $\approx 2-3$ Myr for the most massive stars, ≈ 100 $M_{\odot}$, to ≈ 40 Myr for stars with a mass of $\approx$8 $M_{\odot}$, the least massive stars capable of producing a compact object. In this picture, it would be natural to expect the X-ray binaries in which the compact object is a black hole to appear first and the (probably more abundant) population of accreting neutrons stars to appear next.

On the other hand, the HMXB lifetime is limited by the lifetime of the companion star. Since the least massive companion stars observed during an active X-ray phase have a mass of $\approx 6M_{\odot}$, this lifetime is ~ 60 Myr for a single star when the peculiarities of the stellar evolution in binary systems are disregarded. Given the mass transfer from the more massive star to the future donor star, this lifetime can be slightly modified. This also includes the X-ray source stage proper with characteristic time scales much shorter than those considered above, $\sim 10^3 - 10^6$ yr, depending on the type of the companion star and the binary parameters.

Obviously, the function $\eta_{HMXB}(t)$ must be closely related to the rate of SNe II $\eta_{SNII}(t)$ producing a compact object. To the first approximation, the relation may be assumed to be linear:

$$\eta_{HMXB}(t) = A \cdot \eta_{SNII}(t) \tag{2}$$

The supernova rate can be easily determined from the stellar mass–lifetime relation (Schaller et al. 1992) and the initial mass function (IMF), which below is assumed to be a Salpeter one

in the range 0.1–100$M_\odot$. Note that the IMF shape in the range of low masses is unimportant for us, since all of the relations are eventually normalized to the mass of massive stars with M>8 $M_\odot$. The normalization in Eq. (2) can be calculated using the N_{HMXB}–SFR calibration from Grimm et al. (2003). This relation was derived from Chandra observations of nearby galaxies and corresponds to the time integral of the function $\eta(t)$):

$$\int \eta_{HMXB}(t)dt = \frac{N_{HMXB}(L_X > L_{X,min})}{SFR} \tag{3}$$

As the limits of integration in Eq. (3), we choose 2 and 40 Myr in accordance with the above reasoning.

In what follows, we will compare the experimental dependence $\eta_{HMXB}(t)$ obtained from X-ray and optical SMC observations with predictions of the simple model specified by Eqs. (2) and (3). Clearly, Eq. (2) is based on the assumption that the X-ray phase comes immediately after the formation of a compact object, i.e., it disregards the evolution of the companion star in the binary system. A more rigorous description of the HMXB evolution requires resorting to population synthesis models (see, e.g., Popov and Prokhorov 2004; Belczynski et al. 2005), which is outside the scope of this paper. On the other hand, the experimental dependence $\eta_{HMXB}(t)$, whose derivation is the goal of this paper, can be used by the creators and users of population synthesis models to test and calibrate these models.

1.1. Experimental Determination of the Function $\eta_{HMXB}(t)$

The number of HMXBs observed in a spatial region X at time t is a convolution of the function $\eta_{HMXB}(t)$ with the star formation history SFR(t,X) in this region:

$$N_{HMXB}(t, X) = \int SFR(t - \tau, X)\eta_{HMXB}(\tau)d\tau. \tag{4}$$

Solving the inverse problem formulated by this equation, we can impose constraints on the dependence $\eta_{HMXB}(t)$ from observations. This requires the following:

1. Identifying the HMXB population in the galaxy.

2. Reconstructing the spatially-resolved star formation history SFR(t,X). Obviously, we need only the recent SFH from the current time to the time in the past corresponding to the maximum HMXB lifetime (i.e., $\sim 50 - 100$ Myr).

3. Solving the inverse problem formulated by Eq. (4) given $N_{HMXB}(X)$ and SFR(t,X) for a large set of regions X. Obviously, a galaxy with a rich HMXB population and a SFH that changes significantly from place to place is required to perform this procedure. Because of its proximity and appreciable SFR, the SMC is one of the most natural candidates for such a galaxy. This paper is structured as follows. We describe the SFH reconstruction technique and apply it to the SMC, solve the inverse problem given by Eq. (4), and find the function $\eta_{HMXB}(t)$ for HMXBs in the SMC. Next, we discuss the results obtained and summarize our conclusions.

2. THE STAR FORMATION HISTORY IN THE SMALL MAGELLANIC CLOUD

To reconstruct the SFH, we will use a method based on the analysis of color-magnitude diagrams (see, e.g., Gallart et al. 2005). This method uses the fact that stars of different ages (and metallicities) occupy different positions in the color-magnitude diagram. The SFH can be determined by comparing the distributions of stars in it with predictions of stellar evolution models. Applying this method requires optical photometry at least in two bands. There are several realizations of this method; one of the most commonly used realizations was described by Dolphin (1997), Aparicio et al. (1997), and Dolphin (2002) and consists of the following steps:

1. Generating synthetic color-magnitude diagrams in the required ranges of metallicities and ages on the basis of stellar evolution models. Each diagram is the probability distribution in color-magnitude space for a coeval model stellar population.

2. Correcting the synthetic diagrams for the incompleteness and photometric errors. Allowance for the interstellar extinction and the distance to the galaxy.

3. Approximating the observed color-magnitude diagrams by a linear combination of the derived synthetic models. Estimating the uncertainties of the solution.

Because of their proximity, the Magellanic Clouds are attractive objects for star formation studies. It is not surprising that a number of papers are devoted to the SFH in them (see, e.g., Holtzman et al. 1999; Dolphin 2000). In particular, note the paper by Harris and Zaritsky (2004), who reconstructed the spatially resolved SFH of the SMC. However, in all of these studies, the star formation was considered in a wide range of ages, with the emphasis being inevitably on time scales of $\sim$ Gyr. In contrast, we are interested in the SFH for the youngest stellar population. As will be shown below, its reconstruction has several peculiarities that have escaped attention previously. Therefore, we adapted the SFH reconstruction method to meet the requirements of our problem by concentrating on the time interval 0–100 Myr.

2.1. Synthetic Color-Magnitude Diagrams

The first step in generating synthetic color-magnitude diagrams is to choose the model isochrones that define the region occupied by a coeval stellar population. In what follows, we use the isochrones from Girardi et al. (2002) (the so-called "Padova isochrones") covering wide ranges of ages (log t = 6.60–10.25), metallicities (Z = 0.0001–0.03), and masses (0.15–70 $M_\odot$). All model calculations are performed for the color-magnitude diagrams in (U–B, B) and (B–V , V) spaces.

The theoretical isochrones relate the mass of a star of a certain age to its position in the diagram. Therefore, the probability of filling some region in it can be easily determined

from the corresponding mass interval M_i–M_{i+1} and the IMF, which below is assumed to be a Salpeter one:

$$p(M_i, M_{i+1}) = \frac{M_{i+1}^{-\Gamma} - M_i^{-\Gamma}}{M_{max}^{-\Gamma} - M_{min}^{-\Gamma}}, \quad (5)$$

where $\Gamma = 1.35$, M is the initial mass of the star, M_{min}=0.1 $M_\odot$, and M_{max}=100 $M_\odot$. Note that the IMF deviations from the Salpeter one in the range of low masses affect only the normalization of the derived SFH rather than its shape. This is because we analyze the color-magnitude diagrams only for a relatively massive stellar population. The SFH sensitivity to the IMF deviations from the Salpeter one in the range of high masses is discussed in the Section "Checking the SFH Reconstruction Procedure." Equation (5) allows us to calculate the probabilities of filling various regions in the color-magnitude diagram that are needed to fit the observations by a model. This is convenient to do using model photometry generated by the Monte Carlo method. The total number of model stars must be large enough to minimize the contribution from Poisson noise. In our case, the number of stars is $> 10^5$ per isochrone (which corresponds to 10^8 stars in the mass range 0.1–100 $M_\odot$).

However, before generating model photometry, we must make several more steps, including the choice of an age range, an age step, ametallicity range, a binary fraction and isochrone interpolation. These steps are considered below.

First, we found that the isochrones need to be interpolated. Indeed, the magnitude difference at adjacent points can be 0.5. Therefore, we perform a linear interpolation of the magnitudes in such a way that the magnitude step does not exceed 0.01.

In choosing an age interval and its binning, we will keep in mind that we are interested only in the recent star formation. This allows us to exclude the old population from our analysis and, thus, to avoid problems related to the incompleteness of the optical catalog at faint magnitudes (see the Subsection "Binning of Color-Magnitude Diagrams"). Below, we reconstruct the SFH in the time interval log t = 6.6–8.0. We also include the isochrones in the time interval log t = 8.0–8.6 in our model to avoid the distortion of the solution at log t$\leq$8.0 due to the older population. Initially, the time step in the isochrones is $\Delta \log(t) = 0.05$. The simple tests show that this resolution is excessive in terms of the photometry used (see the Subsection "Optical Photometry"). Therefore, we combine the isochrones into groups, each with 3–4 isochrones, thereby obtaining the time step $\Delta \log(t) = 0.2$.

The binary fraction is also important in generating model stellar populations, since the binary stars in the color-magnitude diagram will appear as single stars with distorted photometry. As the binary fraction, we use the standard value of $f_{binary} = 0.5$. Following Harris and Zaritsky (2004), we will assume that the mass of the companion star is taken from an independent Salpeter IMF. The influence of these assumptions on the derived SFH is discussed in the Section "Checking the SFH Reconstruction Procedure."

2.1.1. Metallicity.

The heavy-element abundance is an important parameter in the evolution of a star. The positions of stars with different metallicities in the color-magnitude diagram will differ almost at all evolutionary stages. For example, since an increase in metallicity is accompanied by an increase in opacity, it causes the main sequence to be displaced toward the less bright and cooler stars. However, metallicity plays the most important role at the final stages of stellar evolution. For instance, the position of a star in the color-magnitude diagram for (super)giants depends critically on the heavy-element abundance. This can give rise, for example, to partial degeneracy between age and metallicity for red supergiants. Therefore, choosing the isochrones with the proper metallicity (or metallicity range) is very important for reconstructing the SFH.

The metal abundance in the Magellanic Clouds is known to be low. For example, the metallicity of the interstellar medium in the SMC is 0.6 dex lower than that of the local medium in our Galaxy (Russell and Dopita 1992). Note also that the SMC metallicity has gradually increased with time due to continuous star formation. Therefore, a self-consistent description of the SFH should take into account the spread in metallicity. Several attempts have been made to describe quantitatively the heavy-element enrichment history of the SMC. The typical metallicities lie in the range from $[Fe/H] \approx -1.25$ (Z$\approx$ 0.001) for the old population to $[Fe/H] \approx -0.5$ (Z$\approx$ 0.006) for the young population (see, e.g., Pagel and Tautvaisiene 1998). Since we are interested in the recent star formation in the SMC, a component relatively rich in heavy elements is expected to dominate among the stellar population used in the calculations. However, a spread in metallicity exists even for the young population (see, e.g., Harris and Zaritsky 2004; Maeder et al. 1999; and references therein). Therefore, to choose the metallicity suitable for the spatial regions used to reconstruct the SFH, we visually compare the observed color-magnitude diagrams with the model isochrones. The effect of the heavy-element abundance is most pronounced for the red supergiant branch. Note that the isochrones in the region of red supergiants in the range $Z \sim 0.004 - 0.008$ under consideration do not intersect, i.e., there is no degeneracy between metallicity and age. We found that the locations of the red supergiant branches in most regions are satisfactorily described by the Z = 0.004 isochrones. However, in one region, the (B–V, V) diagram is described better by Z = 0.008, while Z = 0.004 is more suitable for the (U–B, B) diagram. Below, we use Z = 0.004 everywhere, except for this region where Z = 0.008 is used. We also analyze the dependence of our results on the chosen metallicity (see below).

2.1.2. Interstellar extinction and distance.

The derived synthetic diagrams should also be corrected for the interstellar extinction and the SMC distance. As the distance modulus for the SMC, we take m–M = 18.9 (Westerlund 1997), corresponding to a distance of D$\approx$60 kpc.

Zaritsky et al. (2002) showed that the extinction for the stellar population in the SMC changes from region to region and differs for hot and cool stars and obtained the distributions of extinction for different regions (http://ngala.as.arizona.edu/dennis/smcext.html). We correct the synthetic photometry using these distributions just as was done by Harris

and Zaritsky (2004). For the young stars ($logt < 7.0$), we take the distribution of extinction corresponding to hot stars. For the older population, the distribution of extinction for hot stars is used only for the population fraction $f = 1 - 0.5 \cdot (\log(t) - 7)$, while the fraction 1–f of stars exhibit extinction corresponding to cool stars. Finally, all of the stars older than 1 Gyr have the distribution of extinction corresponding to cool stars.

2.1.3. Photometric errors and completeness.

The synthetic color-magnitude diagrams should take into account the photometric errors and the incompleteness of the optical catalog at low fluxes. The most important source of errors is the telescope's limited resolution. Clearly, the resolution-related photometry distortions depend on the spatial density of stars and will be at a maximum where this density is high. Artificial star tests – reconstructing the photometry of model stars placed on real images through the standard procedures used in compiling a real catalog – are a standard method of solving this problem. The subsequent comparison of the reconstructed photometry with the model one allows the distortions produced by this factor to be estimated as a function of the spatial density of stars. Obviously, this requires input optical data. In addition, there are factors whose contribution is much more difficult to estimate quantitatively (e.g., the systematic uncertainties in the calibration). Analysis of the star catalog used shows that these are actually present (see the Subsection "Optical Photometry"). If the photometric errors are moderately large, then the problem of photometric errors can be solved by choosing a special binning of the color-magnitude diagram, more specifically, using a grid with wider color and magnitude intervals than the characteristic photometry distortions. Since we are interested only in the recent SFH, we can also exclude faint stars for which the problem of photometric errors is more serious. Excluding faint stars also solves the problem with the incompleteness of the catalog. On the other hand, it is clear that we cannot make the cells in the color-magnitude diagram too large, because this can give rise to additional degeneracy in the solution. Since there were no input optical data for the SMC at our disposal, we chose the second path – optimizing the binning of the color-magnitude diagram (for more detail, see the Subsection "Binning of the Color-Magnitude Diagram").

2.2. SFH reconstruction.

Using the synthetic photometry obtained, we can approximate the observed distribution of stars in the color-magnitude diagram (n_i) by linear combinations of model stellar populations ($A_{i,j}$):

$$n_i = \sum_j A_{i,j} \times x_j, \tag{6}$$

where i is the cell number in the diagram and j is the time interval number. The amplitudes x_j minimizing the discrepancy $\|Ax - n\|$ are the sought-for SFH.

Since the problem in question is ill-conditioned, we use an iterative Lucy-Richardson method (Lucy 1974) for its solution. Using the initial approximation to the solution, this

procedure calculates a vector that approaches the maximum likelihood solution with increasing number of iterations. The solution after iteration i is regularized in the sense that the method retains non-negativity of the initial solution and that it is smoother than themaximum likelihood solution. An important feature of the method is the choice of a stopping criterion (Lucy 1994) – the number of iterations giving an optimum solution. Obviously, the stopping criterion is determined by the character of the problem. For example, at low noise in the input data, the maximum likelihood solution is close to the true one, while in the reverse situation with large errors, fitting the data with a high accuracy is equivalent to attempting to describe the noise. Below, we define a stopping criterion suitable for our problem by reconstructing the SFH of a model stellar population and studying the behavior of the likelihood function L depending on the number of iterations (see below):

$$L = \sum_i (\mu - N_i \cdot \ln \mu). \tag{7}$$

2.2.1. Optical photometry.

As the stellar population photometry necessary to reconstruct the SFH, we used the Magellanic Clouds Photometric Survey (MCPS) catalog for the SMC (Zaritsky et al. 2002). To reconstruct the SFH, we use the (U–B, B) and (B–V , V) diagrams. The catalog also presents I-band photometry, i.e., the additional (V–I, I) diagram could be used. However, we found that the I magnitude is often absent (I = 0) for bright stars, with the most significant loss of photometry being observed among the red supergiants. Since the latter play an important role in reconstructing the recent SFH, we decided to exclude the (V–I, I) diagram from our analysis.

Note also the problem with the U photometry of the catalog. As described in Zaritsky et al. (2004), Zaritsky et al. (2002) corrected the U–B color using the photometry from Massey (2002) calibrated (in the initial version) from faint dwarfs. In addition, Zaritsky et al. (2002) replaced part of the photometry for bright stars with the photometry from Massey (2002). As a result, the U–B color for blue supergiants may be unreliable. This is clearly seen in the (U–B, B) diagram as the displacement of the blue supergiant sequence by $\sim 0^m.3$ relative to the model (see, however, the "Section Checking the SFH Reconstruction Procedure" for a discussion of the reliability of stellar evolution models for supergiants). Our binning of the color-magnitude diagram into large cells allows the effect of this kind of uncertainties to be minimized. Therefore, we expect this problem to be not critical in our procedure. Another problem described by Harris and Zaritsky (2004), more specifically, the need for displacing the B-V color by $0^m.1 - 0^m.2$ in some regions, will not affect strongly our results for the same reason. For test purposes, we also used the OGLE catalog (Udalski et al. 1998) containing B, V, I photometry, but covering only part of the SMC.

2.2.2. Contribution from foreground stars.

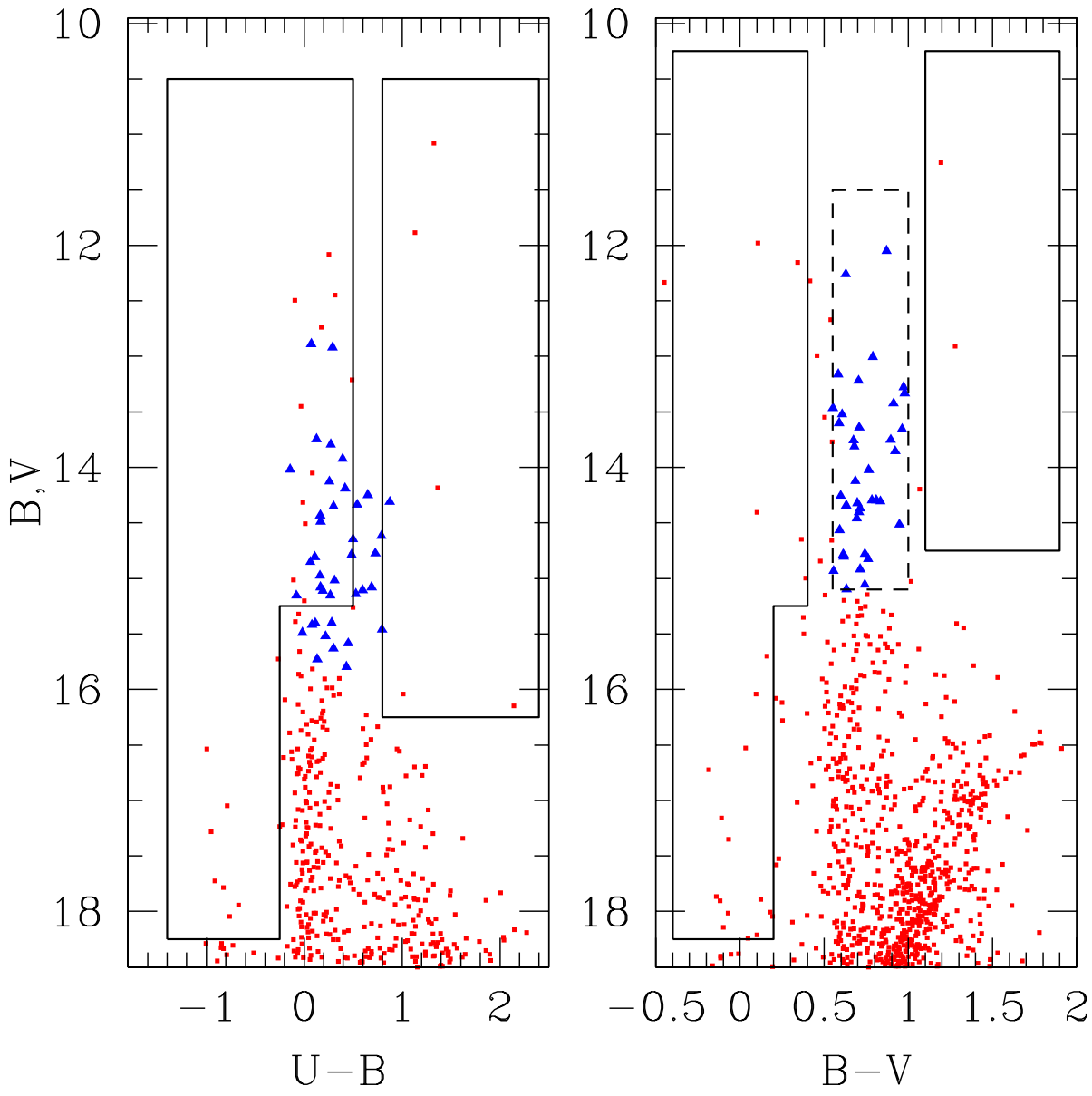

Fig. 1: Color–magnitude diagram for the extreme MCPS fields illustrating the smallness of the contribution from Galactic foreground stars and the efficiency of the method of their rejection. The rectangles (solid line) indicate the regions used to reconstruct the SFH. The dashed line in the (B–V, V) diagram denotes the region that was used to identify foreground stars. The stars that fell into this region are marked by triangles in both diagrams. They were assumed to belong to the Galaxy and were excluded from the analysis in the (U–B, B) diagram.

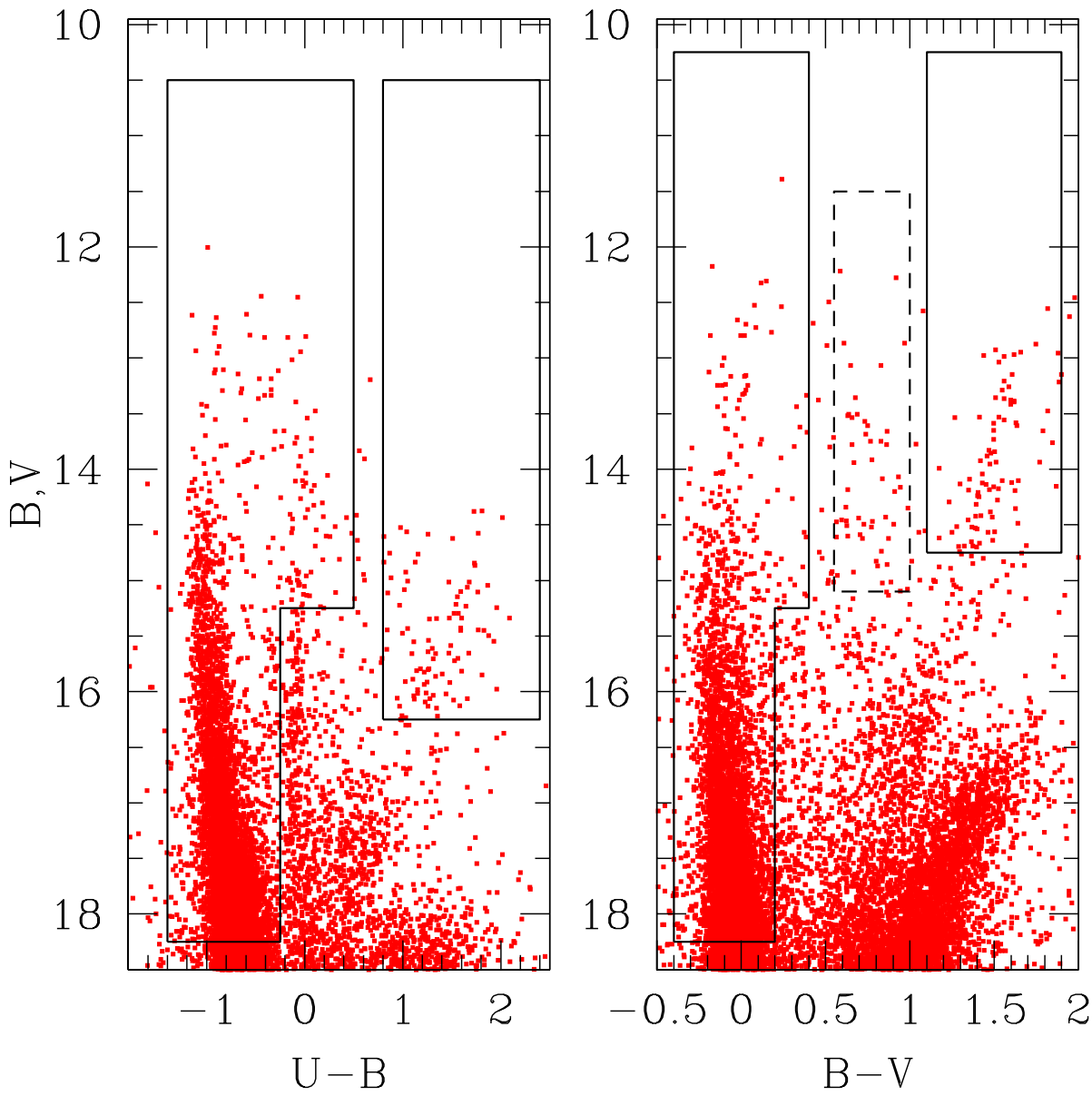

Fig. 2: Color-magnitude diagram for one of the SMC fields used to reconstruct the SFH. The notation is the same as that in Fig. 1.

Obviously, the catalog of stars toward the SMC also contains Galactic stars that can introduce distortions into the color-magnitude diagrams. To estimate their contribution, we constructed the color-magnitude diagrams for 10 outermost MCPS fields (each with an area of $12' \times 12'$) where the contribution from SMC stars is at a minimum (Fig. 1). When comparing the densities of stars in Figs. 1 and 2, we should take into account the fact that the total area of the fields used to construct the diagram for Galactic foreground stars shown in Fig. 1 is approximately twice the area of the sky used to construct the diagram in Fig. 2 (equal to the area of the XMM-Newton field of view). Obviously, the contribution from Galactic foreground stars is negligible in most of the color-magnitude diagram. The only region where Galactic stars can introduce noticeable distortions is the blue supergiant branch in the (U–B, B) diagram in the range of colors near U–B = 0. However, as we see from Fig. 1, they are easily identified in the (B–V, V) diagram, since they are separated from both blue and red supergiants in it. This forms the basis for our foreground star rejection algorithm. We determined the region in the (B–V, V) diagram that, on the one hand, includes most of the Galactic foreground stars superimposed on the SMC blue supergiant branch in the (U–B, B) diagram and, on the other hand, the contribution from SMC stars to it is negligible. This region is highlighted by the dashed line in Figs. 1 and 2. All of the stars lying in this region (they are marked by triangles in both diagrams in Fig. 1) are then excluded from the analysis in both (B–V, V) and (U–B, B) diagrams.

2.2.3. Binning of the color-magnitude diagrams.

To compare the model color-magnitude diagrams with the observations, we must specify their binning. There are two approaches to this problem – uniform and more complex grids. Whereas the former is more objective, the latter makes it possible to avoid problems related to the photometric errors and uncertainties in the stellar evolution. In any case, the choice of a grid must take into account the existence of extended structures corresponding to long stages of stellar evolution in the diagram. The main sequence and blue and red supergiants are most important in determining the recent SFH.

Since the core hydrogen burning is the longest phase of stellar evolution, the number of stars on the main sequence is at its maximum and the latter plays a major role in determining the SFH. In principle, the SFH can be reconstructed based only on the main sequence, without invoking other stages of stellar evolution (see, e.g., Dohm-Palmer et al. 1997). However, this method places heavy demands on the photometric accuracy, because the blue supergiants are close to the upper part of the main sequence (Figs. 2 and 3).

The supergiant branches are important regions in the color-magnitude diagram and complement the main sequence when reconstructing the SFH. However, whereas the evolution of a main-sequence star has been studied well, the evolution of supergiants is more uncertain. This is because the supergiants are very sensitive to such aspects of the model as mass loss, convection, etc. Uncertainties in the latter can strongly affect the manifestation of supergiants in the color-magnitude diagram. The best known outstanding problem here is the blue-to-red supergiant ratio (B/R). As was shown by Langer and Maeder (1995), there are

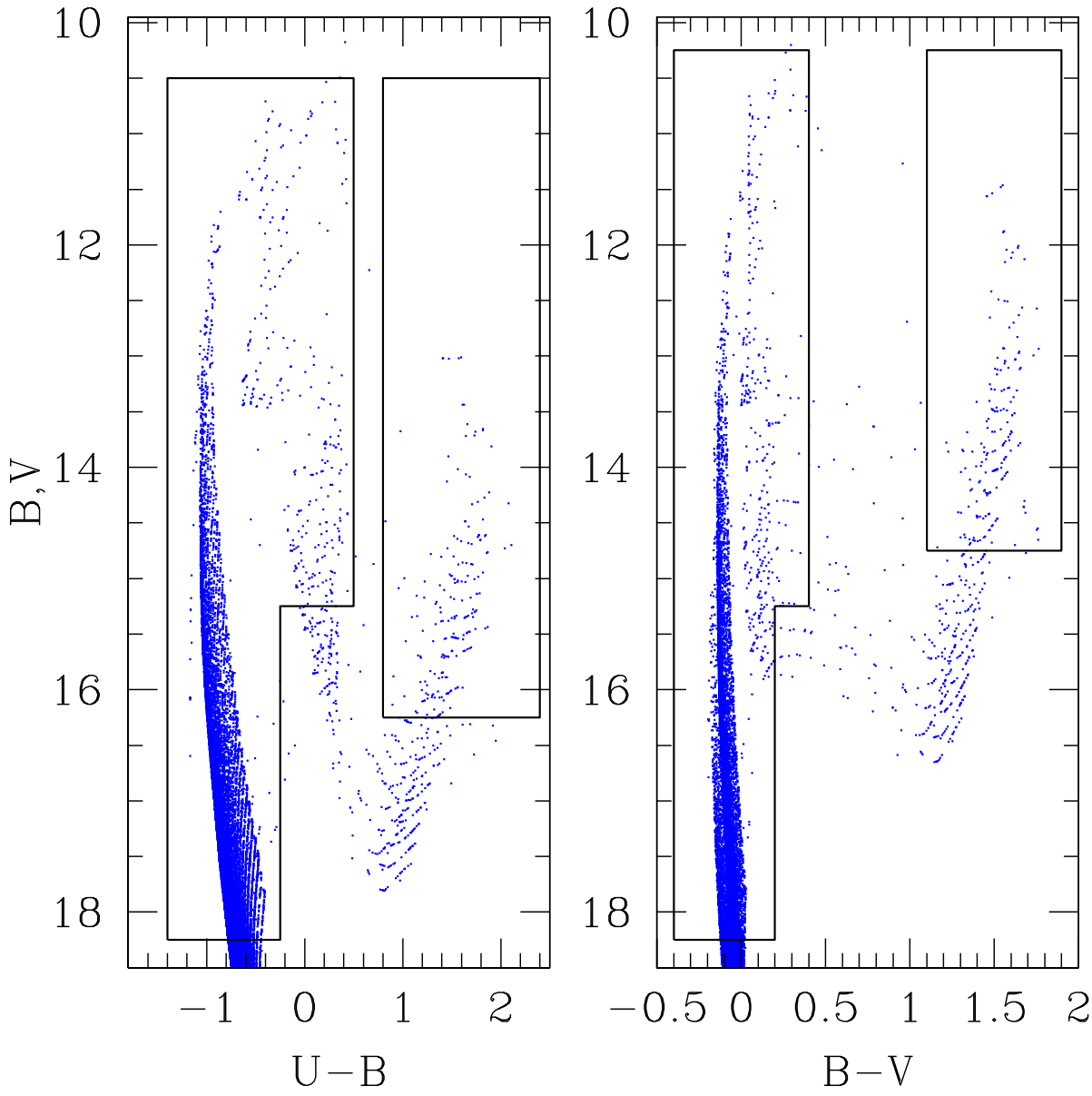

Fig. 3: Synthetic color-magnitude diagram. The rectangles denote the regions used to reconstruct the SFH. The SFH of a model population obeys the law dM/d log t = const in the time interval log t = 6.6–8.0 and is zero outside this interval.

no stellar evolution models that are capable of explaining self-consistently the dependence of B/R on metallicity in a wide range of the latter (see also Gallart et al. 2005).

The region that we use to compare the observations with the model consists of two strips: one covers the main sequence and the blue supergiant branch and the other covers the region of red supergiants (see Fig. 3). The width of each strip is taken to be much larger than the scatter in photometry, which also allows the effect of uncertainties in the stellar evolution models to be reduced (for more detail, see the Section "Checking the SFH Reconstruction Procedure"). At the same time, it is small enough for the contribution from Galactic foreground stars to be at a minimum (Fig. 1). Since each strip has only one color interval, using this grid is equivalent to simultaneously fitting two luminosity functions. The scatter in magnitude is less important than the scatter in color, because all of the features in the color-magnitude diagram are elongated along the magnitude axis. Its effect is equivalent to convolving the SFH with the function defined by the distribution of photometric errors. We take dm = 0.25 as the width of the magnitude interval.

The magnitude threshold for the main sequence was chosen to be V_{lim}=18.25 and B_{lim}=18.25. This allowed us to avoid problems with the incompleteness of the catalog and with the photometry distortion through the superposition of stars. Indeed, for the MCPS catalog, the completeness is large for $\sim 20^m$ stars and the magnitude errors (including the star superposition effect) for bright stars are smaller than the chosen width of the color and magnitude intervals (Zaritsky et al. 2002). We used a higher threshold for red supergiants to avoid the contribution from the old low-metallicity stellar population.

2.2.4. Uncertainty of the solution.

To estimate the statistical uncertainty in the reconstructed SFH, we analyzed the stability of our solution to Poisson noise in the number of stars by the bootstrap method. We calculated the expected number of stars in each cell in the color-magnitude diagram from our solution. Next, we drew their realization by assuming a Poisson distribution for the number of stars, which was then used as input data in the SFH reconstruction code. This procedure was repeated many times and the rms scatter of the solutions obtained was taken as the error.

2.3. Checking the SFH Reconstruction Procedure.

To check the SFH reconstruction procedure, we performed a number of tests. First of all, to check the general functioning of the algorithm and its implementation, we reconstructed the SFHs for various model stellar populations. Subsequently, we investigated the adequacy of the stellar evolution models and the accuracy with which the observed color-magnitude diagrams are approximated. Finally, we analyzed the stability of the solution to photometric errors and its sensitivity to various model parameters, such as the metallicity, the binary fraction, and the IMF slope.

Reconstructing the SFH for a model stellar population.

For the first test, we chose a model stellar population whose SFH consists of several bursts alternating with periods of quiescence. The number of stars in the model population was close to that observed in the SMC within the XMM-Newton field of view. This test allows us to check the SFH reconstruction procedure, the degeneracy between adjacent time intervals, and to analyze the dependence of the solution on the stopping criterion in the Lucy-Richardson method. The results are presented in Fig. 4, which shows the behavior of the likelihood function depending on the number of iterations and the model and reconstructed SFHs. We compare two solutions – one long before the saturation of the likelihood function (200 iterations) and the other close to its saturation (1000 iterations). Obviously, the latter corresponds much better to the model.

The model SFH used in the first test is implausibly complicated. As a more realistic example, we chose the actual SFH obtained for one of the SMC fields and used the model stellar population corresponding to it as input data in our code. As we see from Fig. 4, the model SFH is smoother in this case. As in the previous case, the best solution is achieved close to the saturation of the likelihood function.

Based on the results of these and other tests, we concluded that the best solution is achieved near the saturation of the likelihood function. In other words, the problem has such a character (the number of stars etc.) that the solution obtained requires no (or almost no) significant regularization.

The adequacy of stellar evolution models.

To verify the adequacy of the model isochrones, we analyzed how well the model describes the color-magnitude diagram for the actual stellar population. Figure 5 presents the model and observed luminosity functions for themain sequence with blue supergiants and for red supergiants summed over all of the SMC fields used in this paper. These luminosity functions correspond to the two regions shown in Fig. 2. We see that the model agrees well with the observations for faint magnitudes, but in the region of bright stars ($B, V \lesssim 13.5$) the model prediction for the main sequence and blue supergiants exceeds appreciably the observations. As our tests showed, this excess is related to blue supergiants – the two clearly seen features in the model luminosity function at V$\approx$13 and $\approx$ 11.5, which are much less pronounced in the data, are unequivocally identified with them. This is clear from an examination of the color-magnitude diagram for the model population in the (U–B, B) diagram in Fig. 3. The problem with the excess for the brightest stars can be partly removed if the metallicity is assumed to be Z = 0.008 for all fields. In this case, however, the locations of the supergiant branches in the color-magnitude diagram will be in poorer agreement with the data. On the other hand, the luminosity function for red supergiants is described well by the model. Obviously, the discrepancy between the data and the model results from uncertainties in modeling the supergiants, whichmanifest themselves as the problem of the blue-to-red supergiant ratio mentioned above.

To estimate how strongly this affects the reconstructed SFH, we analyzed the sensitivity

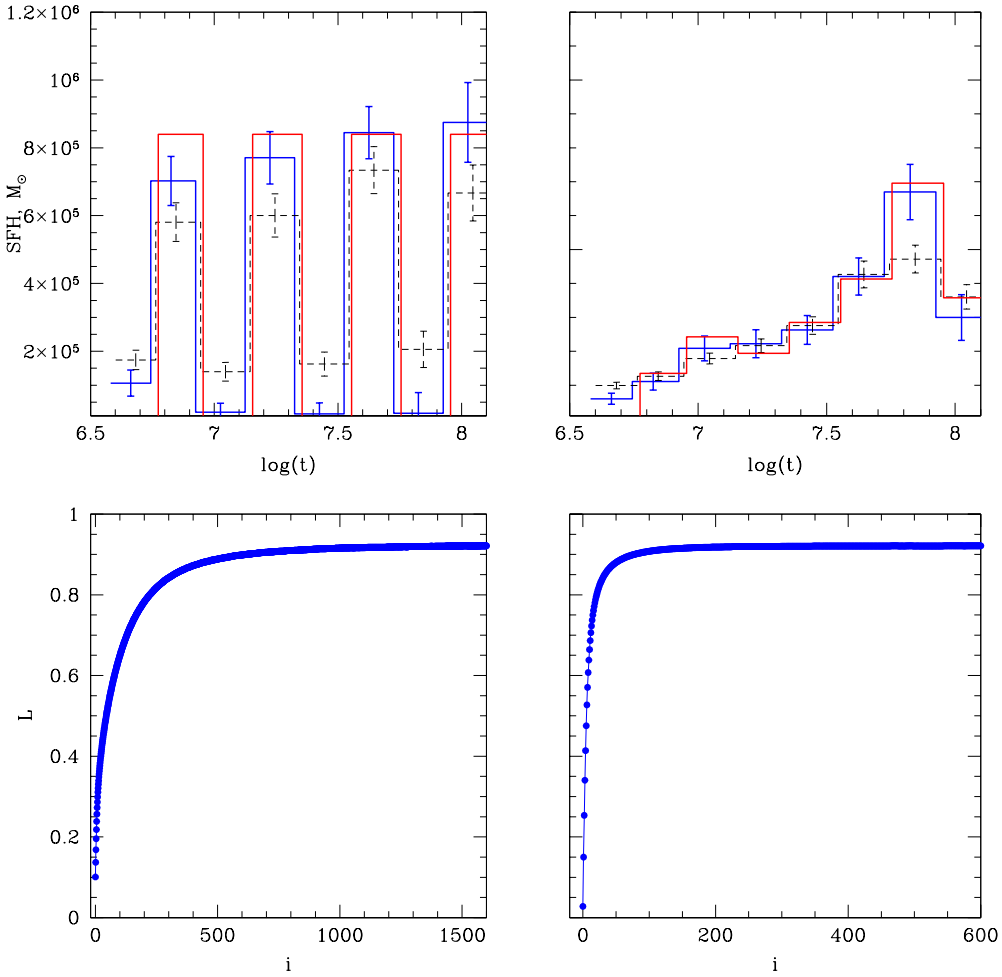

Fig. 4: (a), (b) Reconstructed SFHs for model stellar populations. The mass formed in different time intervals is along the vertical axis. The model SFH is indicated by the thick line without error bars. For clarity, the histograms were displaced along the time axis. (c), (d) Behavior of the likelihood function for the solution depending on the number of iterations in the Lucy-Richardson method. Model is a series of star formation events alternating with periods of quiescence (a) and the SFH in one of the SMC fields (b). The solid and dashed histograms indicate the solutions obtained by the Lucy-Richardson method after 1000, 200 (a) and 250, 40 (b) iterations, respectively.

of the solution to the choice of stellar evolution models and metallicity, more specifically, we reconstructed the SFH using the Padova isochrones with Z = 0.004 and Z = 0.008 and the Geneva isochrones (Charbonnel et al. 1993) with Z = 0.004. The latter use the same convection criterion as the Padova ones. However, as was pointed out by Langer and Maeder (1995), they give different predictions for the occurrence frequency of supergiants. A visual comparison of the two model populations showed that the locations of the supergiant branches in the color-magnitude diagram predicted by the Geneva isochrones differ significantly from those predicted by the Padova isochrones. As we see from Fig. 6a, the solutions obtained with these two models also differ from one another. Since the observed diagrams are described by the Padova isochrones much better, the solution obtained with the latter is probably more realistic and below we take it as the main one. A similar situation is also observed for the solutions obtained with the same (Padova) isochrones, but with different metallicities – they are statistically incompatible with one another, although the differences are appreciably smaller than than in the case of different stellar evolution models (Fig. 6b). The general tendency in the behavior of the solution is retained, because the main constraints on the SFH are imposed by the distribution of stars along the main sequence, on which the stellar evolution is modeled much better than on the supergiant branches. As a result of the model inadequacy, the solution also slightly depends on the choice of the region under consideration in the color-magnitude diagram. This is illustrated by Fig. 6b, which shows the solution on a grid with a more stringent magnitude threshold for supergiants. As we see from Fig. 6, the solutions differ, but less than in the previous cases.

As has already been noted above, we could reconstruct the SFH using only main-sequence stars, thereby avoiding the supergiant-related problems. However, the accuracy of the photometry available at our disposal is insufficient for the latter to be reliably separated from the main-sequence stars.

Thus, imperfectness of the models for massive stars on which the present stellar evolution models are based limits the reconstruction accuracy of the recent star formation history. Only the general behavior of the SFH has a reasonable accuracy, while the individual features in it should be interpreted with caution. To minimize the effect of such uncertainties, below we coarsen the grid in time by combining two time bins into one. As a result, four of them remain in the interval log t = 6.6–8.0 instead of eight. As we see from Fig. 7, although this does not solve all of the problems considered above, it allows the uncertainties in the solution related to them to be reduced appreciably. As will be clear in the subsequent analysis, a higher time resolution is not required for the problem under consideration, because the accuracy of determining the sough-for function $\eta_{HMXB}(t)$ is limited by the Poisson noise associated with the relatively small number of HMXBs in the SMC.

It is interesting to compare the SFH that we obtained with that from Harris and Zaritsky (2004), whose method differs significantly from ours. It should be kept in mind that Harris and Zaritsky (2004) investigated the SFH in a wide range of ages and did not concentrate on the features related to the reconstruction of recent star formation. The two SFHs are shown in Fig. 7a. We see that they are in satisfactory agreement at $t \gtrsim 20$ Myr and differ on shorter time scales. The largest discrepancy is observed in the second time bin

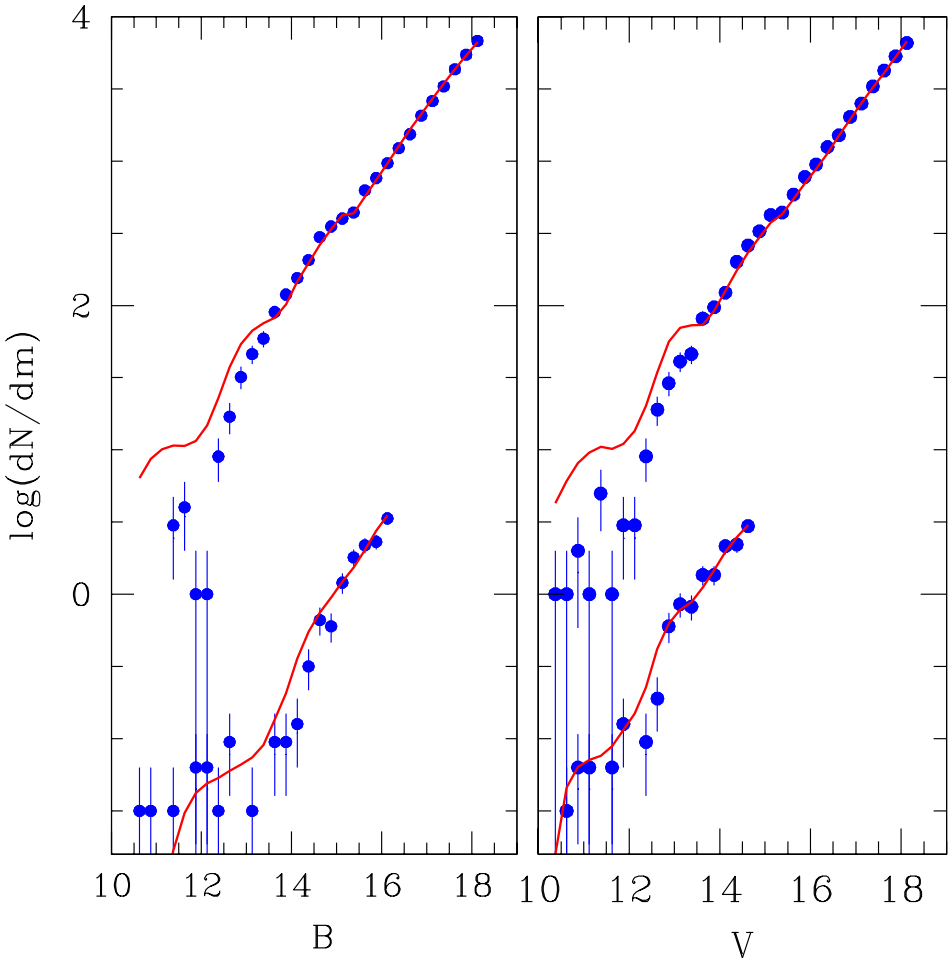

Fig. 5: Luminosity functions for the stellar population in the SMC for the main sequence and blue supergiants (the points with error bars and the curves in the upper part of the plots) and red supergiants (in the lower part of the plots). The points with error bars represent the observed luminosity function; the curve represents their best fits. For clarity, the red supergiant branches were displaced along the horizontal axis. The excess of the model for the main sequence and blue supergiants above the data in the region of bright stars results from inaccuracy of the currently available stellar evolution models for supergiants.

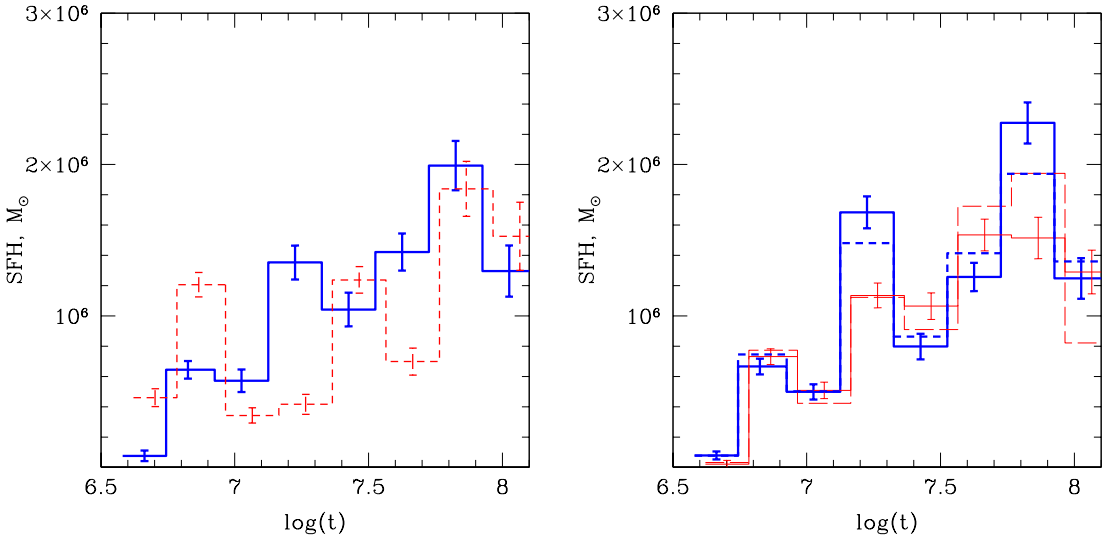

Fig. 6: (a) Dependence of the solution on the choice of stellar evolution models. The solid and dashed histograms correspond to the solutions obtained from the Padova and Geneva isochrones, respectively. Note that the Padova isochrones describe the distribution of supergiants in the color-magnitude diagram much better. (b) Demonstration of the sensitivity of the solution to metallicity and binning of the color-magnitude diagram. The solid thick and thin histograms correspond to the solutions obtained from the Padova isochrones on themain grid with Z = 0.008 and 0.004, respectively. The thick dashed (short dashes) and thin (long dashes) histograms correspond to the solutions obtained with an increased threshold for supergiants and the same metallicities.

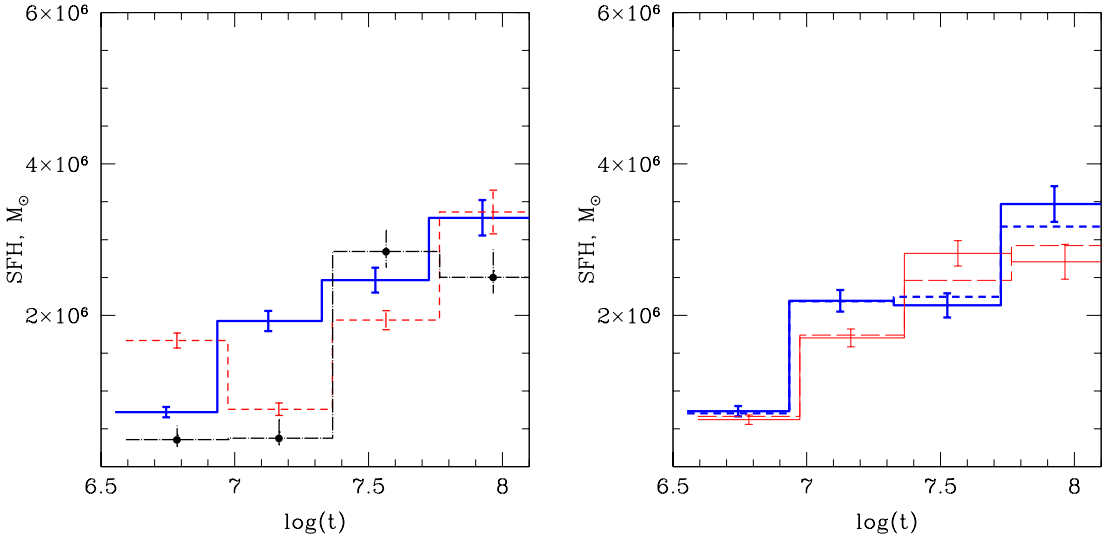

Fig. 7: Same as Fig. 6 constructed in wider time bins. Clearly, the problems obvious in Fig. 6 become less prominent in the solution with a rougher time resolution. The dash-dotted histogram represents the SFH from Harris and Zaritsky (2004).

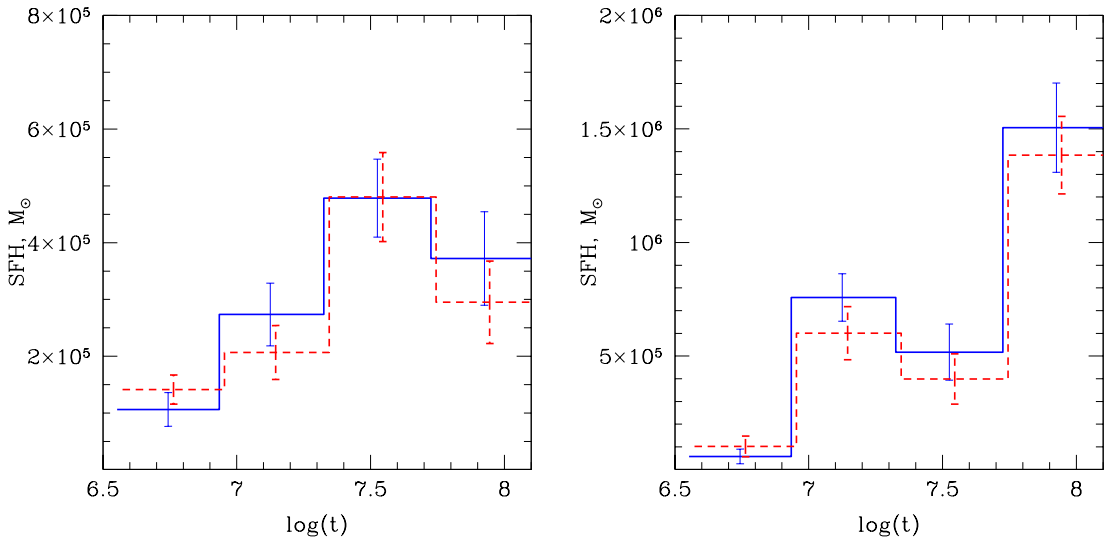

Fig. 8: Demonstration of the sensitivity of the solution to photometric errors. (a) SFH for the actual stellar population in one of the SMC fields (solid histogram) and the same population with photometry distorted by random errors distributed uniformly in the interval -0.2–0.2 (dashed histogram). (b) SFH in one of the fields reconstructed using the MCPS (solid histogram) and OGLE (dashed histogram) catalogs.

corresponding to $\log(t) \approx 7.0 - 7.3$. For a quantitative comparison of the accuracies of the two SFHs, let us consider the number of red supergiants formed in this time bin predicted by these two dependences. The stars formed in the bin $\log(t) \approx 7.0 - 7.3$ that have become red supergiants by now had initial masses in the range $\approx 12 - 22 M_{\odot}$. Their current positions in the color-magnitude diagram are roughly limited by the intervals of magnitudes V = 12.0–13.5 and colors B–V=1.4–1.8. The SFH obtained in this paper predicts 57 stars in these magnitude and color intervals, while according to Harris and Zaritsky (2004), their number must be 15. The numbers of stars are shown for the set of all fields for which the SFH was obtained in Fig. 7. As would be expected, the predictions differ by almost a factor of 4. We emphasize that both solutions are based on the same stellar evolution models and identical assumptions about the IMF, the binary fraction, and the stellar mass distribution in binary systems. These numbers should be compared with the observed number of red supergiants, 50. Obviously, the solution obtained in this paper describes better the population of massive young stars. Since the mass of the stars formed in this time bin is low, this difference affects weakly the end result, as we demonstrate below.

Stability of the solution to photometric errors.

To verify that the solution is only weakly sensitive to photometric errors, we performed two tests. In the first test, we introduced noise into the actual photometry by shifting the magnitudes by random values distributed uniformly in the interval from -0.2 to +0.2. Subsequently, we reconstructed the SFH using the original and distorted photometries. As is clear from Fig. 8, the solution depends weakly even on such large errors. As the second test, we compared the SFHs for the actual stellar population obtained using two different catalogs,

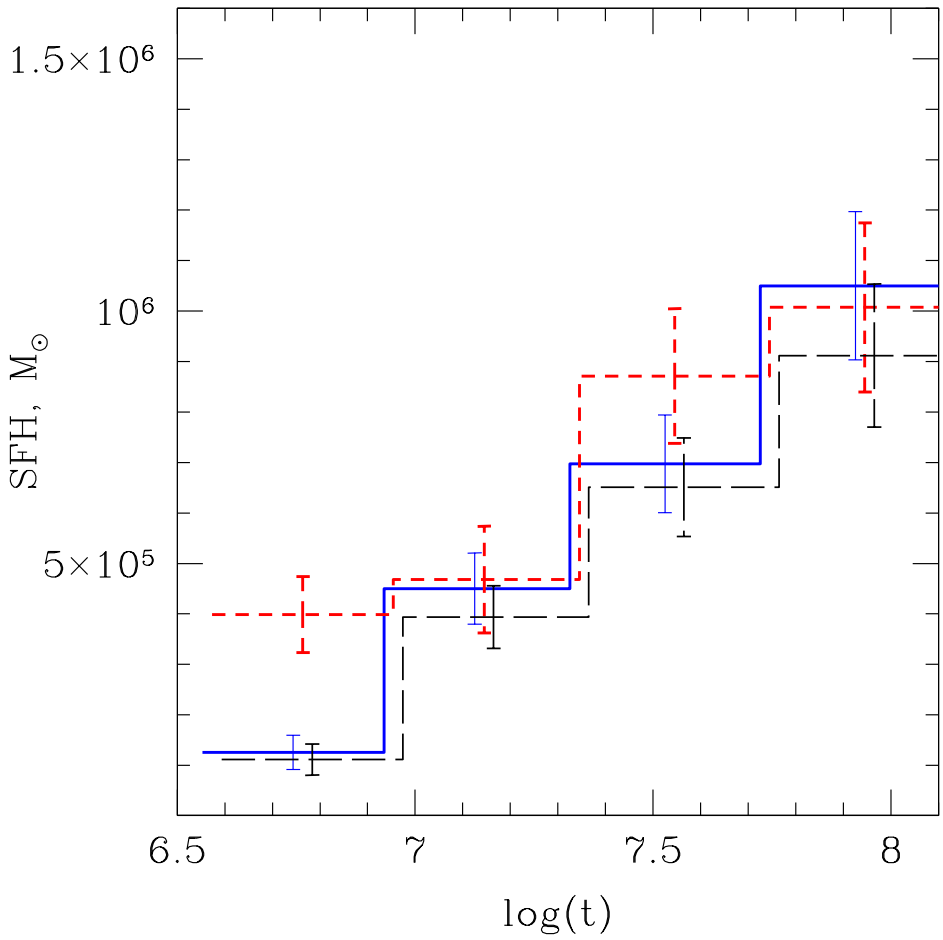

Fig. 9: Demonstration of the dependence of the solution on IMF and distribution in binary component mass ratio. The solid histogramrepresents the solution obtained with standard parameters; the histograms with long and short dashes represent the solutions obtained by assuming a flat distribution in mass ratio and an IMF with a slope of 2.7, respectively. In the latter case, the normalization was reduced by a factor of 2.

OGLE and MCPS. Since the OGLE catalog provides photometry only in the B, V, I bands, we use only the (B-V, V) diagram. Obviously, this procedure is equivalent to reconstructing the SFH for one stellar population with the errors taken from different distributions. The derived SFHs are in good agreement with one another (Fig. 8).

Dependence of the solution on IMF, binary fraction, and binary component mass ratio.

In constructing the synthetic color–magnitude diagrams, we assumed a Salpeter IMF. Since we use only the upper part of the color-magnitude diagram, only the behavior of the mass function for massive stars is important to us. Although the stellar mass distribution in (massive) star clusters is known to follow the Salpeter mass function up to the highest masses, the mass function of the field stars may be steeper (Massey 2003). To check how strongly the solution depends on the presumed IMF slope, we reconstructed the SFH in

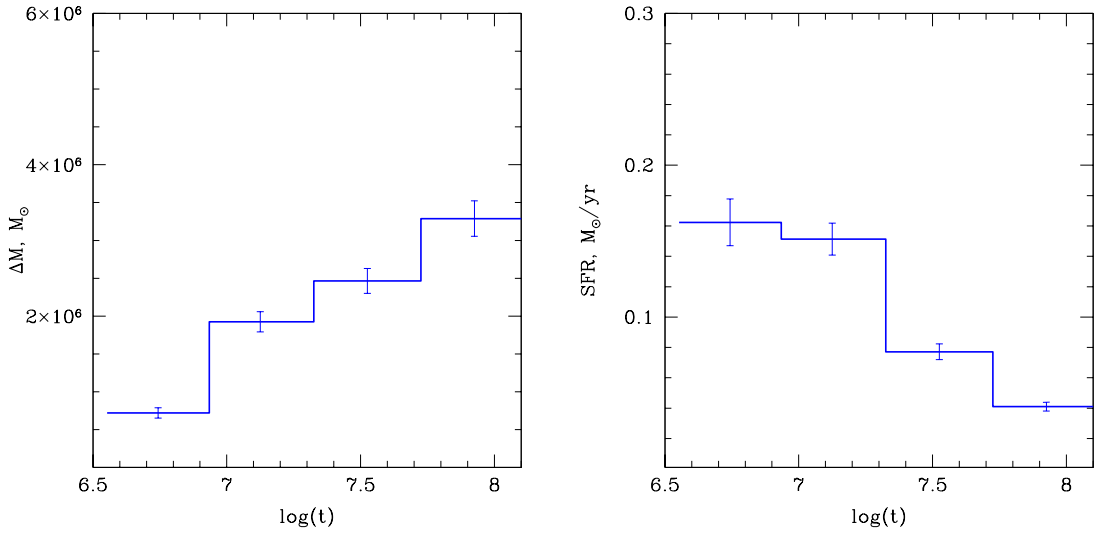

Fig. 10: Combined SFH in the eight SMC regions used to reconstruct the dependence $N_{HMXB}(t)$. The mass (a) formed in different time intervals and the SFR (b) are plotted along the vertical axes as functions of time.

one of the SMC fields by assuming a steeper slope, $\Gamma = 1.7$. The derived SFH does not differ greatly from the solution obtained with the standard value of $\Gamma = 1.35$, except that its normalization is a factor of 2 higher (see Fig. 9). Formally, this difference stems from the fact that we assume the same IMF slope in the entire mass range $0.1 - 100 M_{\odot}$. The end result of our calculations will be virtually unchanged, since it was normalized to the total mass of the massive stars $M > 8\ M_{\odot}$, while the difference of the normalization is attributable to the low-mass stars.

In generating the synthetic diagrams, another significant assumption is made with regard to the fraction of binary systems and their distribution in mass ratio. The binary fraction can exceed f_{binary}=0.5 adopted here as the standard one, while the distribution in binary component mass ratio is nearly flat (see, e.g., Kobulnicky et al. 2006). To analyze the dependence of the solution on these assumptions, we reconstructed the SFH for one of the fields by assuming that the distribution in component mass ratio is flat and that all stars are in binaries (f_{binary}=1). In both cases, the solution is found to be close to that obtained with standard parameters (see Fig. 9; the solution with a different binary fraction is not provided, since it is almost identical to the standard one). However, the conversion coefficient from the number of stars to the stellar mass depends on these parameters. Therefore, the normalization of the derived SFH may differ. Thus, for example, the SFH normalization for f_{binary}=1 increases by a factor of ≈ 1.3.

2.4. Results: The SFH in the SMC

Based on the results of previous sections, we reconstructed the SFH in the SMC. This was done separately for each of the regions observed with XMM-Newton and used in Shtykovskiy

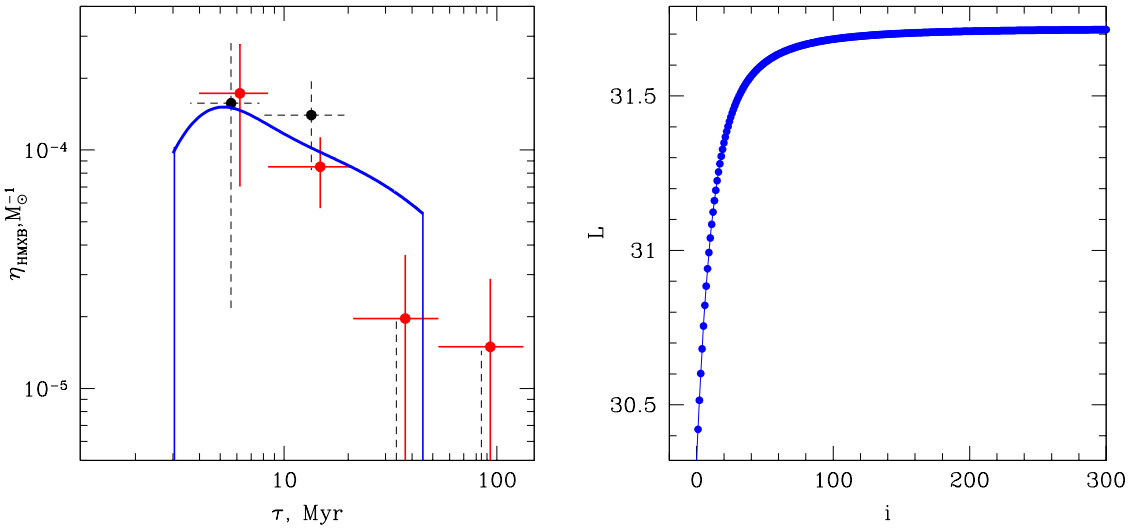

Fig. 11: Demonstration of the reconstruction of themodel dependence of the HMXB number on the time elapsed since the star formation event. (a) The model (solid line) and the solutions obtained by the Lucy-Richardson method after 20 (solid crosses) and 100 (dashed crosses) iterations. (b) Likelihood function of the solution versus number of iterations.

and Gilfanov (2005b) to search for HMXBs. The pointing at CF Tuc, which is displaced considerably from the SMC center and contains no HMXBs, constitutes an exception. The combined SFH for these regions is shown in Fig. 10.

3. EVOLUTION OF THE HMXB POPULATION AFTER THE STAR FORMATION EVENT

Having the spatially resolved star formation history SFR(t,X), let us turn to the solution of Eq. (4). To construct the function $N_{HMXB}(t, X)$, we used our catalog of HMXBs in the SMC (Shtykovskiy and Gilfanov 2005b), from which we selected HMXBs brighter than 10^{34} erg/s. This threshold corresponds to the detection of ≈75% of the sources (see Shtykovskiy and Gilfanov 2005b). To take into account the incompleteness of the catalog, we will divide our solution $\eta_{HMXB}(t)$ by 0.75. The spatial variable X in Eq. (4) is basically the index numbering the XMM-Newton fields of view – Eq. (4) is written for each pointing.After discretization, we obtained a system of eight linear equation for four unknowns. The number of unknowns is determined by the number of time bins in the interval log t = 6.6–8.0. As above, we used the iterative Lucy–Richardson method to obtain a regularized solution. To find the stopping criterion, we solved the problem based on the model function $\eta(t)$. Using the SFHs SFR(t,X) and the function $\eta(t)$ based on the SN II rate, we calculated the expected numbers of HMXBs in eight spatial regions in the SMC and their Poisson realizations. The total number of model sources is close to the actual number of HMXBs in the SMC. The reconstructed dependence $\eta(t)$ is shown in Fig. 11 for two stopping criteria; one is close to the plateau in the likelihood function (100 iterations) and the other is long before it (20 iterations). As we see from the

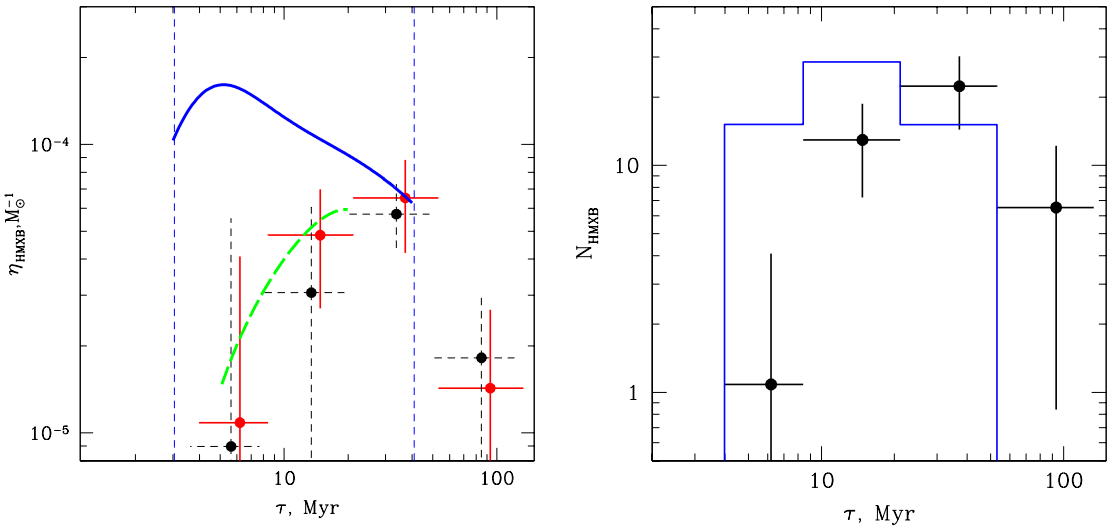

Fig. 12: (a) Dependence of the HMXB number on the time elapsed since the star formation event. The solid and dashed crosses were obtained using the SFH reconstructed in this paper and the SFH from Harris and Zaritsky (2004). The solid curve represents the model based on the supernova rate. The two vertical dashed lines reflect the formation times of the first black hole and the last neutron star calculated in terms of the standard theory of evolution of a single star. The dashed curve represents the theoretical dependence of the number of Be/X systems with neutron stars from Popov et al. (1998). (b) The age distribution of HMXBs in the SMC. The points with error bars were obtained by multiplying the data of the observational curve (a) by the mass formed in the corresponding time bins. The histogram reflects the predictions of the model based on the supernova rate. Obviously, the observed number of the youngest systems is appreciably lower than the predicted one.

figure, the latter is in better agreement with the model and, in addition, has smaller errors. This means that the problem is ill-posed and its solution requires regularization.

4. RESULTS AND DISCUSSION

The derived dependence of the HMXB number on the time elapsed since the star formation event, $\eta_{HMXB}(t)$, is shown in Fig. 12a. The uncertainty of the solution was calculated in the same way as above in the Subsection "Uncertainty of the Solution". To take into account the incompleteness of the catalog of HMXBs in the SMC, we multiplied the normalization of the solution obtained by the factor 1.3. The theoretical curve in Fig. 12a corresponds to the model based on the SN II rate and normalized using the N_{HMXB}–SFR calibration (Grimm et al. 2003), as described in the Section "Evolution of the HMXB Population after the Star Formation Event". The solutions shown in Fig. 12a were obtained both for the SFH determined in this paper and for the SFH from Harris and Zaritsky (2004). We see that the solutions are compatible, despite a certain difference between the two SFHs in the lower time bins (Fig. 7) – as was mentioned above, the accuracy of the solution is limited by the Poisson noise due to the relatively small number of HMXBs in the SMC.

As is clear from Fig. 12a, the HMXB formation efficiency does not exceed the prediction based on the mean N_{HMXB}–SFR relation for the local Universe. The abundance of HMXBs in the SMC is the result of a specific form of the recent SFH in this galaxy, namely, its high rate ~ 50 Myr ago.

The specific form of $\eta_{HMXB}(t)$ differs significantly from the behavior of the SN II rate: the HMXB number reaches its maximum 20–50 Myr after the star formation event, i.e., on time scales of the order of or longer than the explosion time of the last supernova with the formation of a neutron star. Note also the paucity of the youngest systems compared to the model predictions. Obviously, most of the young systems correspond to HMXBs with black holes, since they are the first to be formed after the star formation event. This shortage is not unexpected from an observational point of view, since most of the HMXBs in the SMC are known to be pulsars with Be companions. However, it is of great interest from the standpoint of the theory of formation and evolution of binary systems. Obviously, this behavior is related to the evolution of a companion star whose lifetime can reach ~ 60 Myr for a single $6M_{\odot}$ star (when the evolution effects in the binary system are disregarded). Another important factor is the evolution of the neutron star spin period (Illarionov and Sunyaev 1975). Population synthesis models are an adequate tool for studying these effects. As an example, Fig. 12a shows the time dependence of the number of Be/X systems with neutron stars derived by Popov et al. (1998) based on calculations using the "Scenario Machine". The systems of other classes (e.g., neutron stars with supergiants) are much less numerous, given the luminosity threshold of 10^{33} erg/s chosen by the authors. Therefore, we provide no curves for them. To be able to compare the absolute number of Xray sources with the results of our observations, we renormalized the theoretical dependence to the number of systems brighter than 10^{34} erg/s. For this purpose, we used the luminosity function for HMXBs in the SMC obtained previously (Shtykovskiy and Gilfanov 2005b). Note that its slope in the range of

low luminosities is slightly smaller than the standard value of 0.6 (Grimm et al. 2003). As we see from Fig. 12a, there is good agreement with the observations both in the shape of the dependence and in its normalization in the time interval 5–20 Myr in which the models by Popov et al. (1998) are valid. Note that Popov et al. (1998) performed their calculations by assuming a solar heavy-element abundance, while the details of the population of X-ray sources depend on metallicity (Dray 2006). Obviously, our experimental dependence can be used to test and "calibrate" the population synthesis models and to clarify the various aspects of the evolution of binary systems.

Figure 12b shows the age distribution of HMXBs in the SMC, which is the product of the reconstructed dependence $\eta_{HMXB}(t)$ by the mass of the stars formed in the corresponding time bins. As is clear from Fig. 12b, the HMXB population in the SMC is rather old, $\tau \approx 20 - 50$ Myr. Dray (2006) also reached a similar conclusion by analyzing the observed distributions of HMXB periods and luminosities and by comparing them with the results of population synthesis models. She also suggested the existence of a relatively recent intense star formation event in the SMC.

When the results shown in Fig. 12 are interpreted, it should be kept in mind that we used X-ray sources with luminosities $L_X \geq 10^{34}$erg/s, i.e., faint sources dominate in our sample, to reconstruct the time dependence of the HMXB number. It would be interesting to look at the behavior of the function $\eta_{HMXB}(t)$ for bright sources, e.g., $L_X \gtrsim 10^{37}$erg/s. Indeed, although the luminosity of a specific binary depends on the size of its orbit, one may expect its mean X-ray luminosity to rise with increasing mass of the companion star. Bright X-ray binaries will then be, on average, younger than faint ones due to the shorter lifetime of more massive stars. This conclusion is also supported by the observational fact that brighter sources in star-forming galaxies are, on average, closer to young star clusters (see, e.g., Kaaret al. 2004). Therefore, the time dependence of the number of bright sources will differ from that shown in Fig. 12. However, such a study cannot be performed for the SMC because of its insufficiently high SFR and, accordingly, small number of bright sources. Note also that the N_{HMXB}–SFR and L_X–SFR relations from Grimm et al. (2003) are based on Chandra observations of bright HMXBs in other galaxies. Therefore, one might expect these relations to break down for a lower luminosity threshold. This effect will be unimportant for the L_X–SFR relation, since the total X-ray luminosity of the HMXB population is determined mainly by bright sources in view of the shape of their luminosity function. However, the total number of sources is determined by the more numerous faint sources. Therefore, one might expect noticeable deviations from a linear relation in the N_{HMXB}–SFR relation when the luminosity threshold is lowered.

5. CONCLUSIONS

We considered the relation between the HMXB population and the SFH of the host galaxy. The number of HMXBs can be represented as a convolution (Eq. (4)) of the star formation history SFR(t) with the function $\eta_{HMXB}(t)$ describing the dependence of the HMXB number on the time elapsed since the star formation event. Thus, the evolution of

the HMXB population after the star formation event can be reconstructed by analyzing the distribution of HMXBs in stellar complexes with different SFHs.

Using archival optical observations, we reconstructed the spatially resolved SFH in the SMC over the past ∼100 Myr (Fig. 10). For this purpose, the observed color-magnitude diagrams of the stellar population were approximated by linear combinations of model isochrones. We analyzed the stability and errors of this method for reconstructing the recent SFH and showed that its accuracy is limited by the uncertainties in the currently available models for the evolution of massive stars. However, the systematic error introduced by this factor may be ignored, since the main source of uncertainty in the solution is the Poisson noise due to the relatively small number of HMXBs in the part of the SMC investigated by XMM-Newton.

Using the derived SFHs and the spatial distribution of HMXBs in the SMC from Shtykovskiy and Gilfanov (2005b), we reconstructed the function $\eta_{HMXB}(t)$ that describes the dependence of the HMXB number on the time elapsed since the star formation event (Fig. 12). We compared the derived dependence with the behavior of the SN II rate. The HMXB number reaches its maximum ∼20–50 Myr after the star formation event, which is comparable to or exceeds the lifetime of a $8M_{\odot}$ star. This is much later than the maximum of the SN II rate. In addition, note the shortage of the youngest systems. Observationally, this manifests itself in the absence (or an extremely small number) of HMXBs with black holes in the SMC. This behavior is related to the evolution of the companion star and the neutron star spin period and is consistent with the population synthesis model calculations (Popov et al. 1998). When these results are interpreted, it should be kept in mind that the function $\eta_{HMXB}(t)$ depends on the luminosity threshold used to select the X-ray sources. In our analysis, we used a sample with a low luminosity threshold, $L_{min} \sim 10^{34}$ erg/s. In such a sample, low-luminosity sources, mostly Be/X systems, mainly contribute to the number of sources, while the relative contribution from systems with black holes and/or O/B supergiants, which must constitute the majority of sources in the lower time bin in Fig. 12, is small. Therefore, the time dependence of the number of bright sources (e.g., $> 10^{37}$ erg/s) will differ from that shown in Fig. 12.

The HMXB formation efficiency in the SMC does not exceed the prediction of the N_{HMXB}–SFR calibration (Grimm et al. 2003). Their abnormal abundance compared to the predictions based on the emission in standard SFR indicators, such as the H_{α} line, can result from a peculiarity of the SFH in the SMC.

ACKNOWLEDGMENTS

P.E. Shtykovskiy thanks the European Association for Research in Astronomy (EARA; MESTCT-2004-504604) for support by a Marie Curie fellowship and the Max-Planck-Institut fur Astrophysik, where much of this work was performed, for hospitality. This work was also supported by grant no. NSh-1100.2006.2 from the President of Russia and the Russian Academy of Sciences ("Origin and Evolution of Stars and Galaxies" Program). We thank

the referees for valuable remarks that helped to noticeably improve the presentation of our results in the paper.

References

Aparicio, A., Gallart, C., Bertelli, G., Astron. J. 114, 680 (1997).

Belczynski, K., Kalogera, V., Rasio, F.A. et al. (astro-ph/0511811) (2005).

Westerlund, B., "The Magellanic Clouds", Cambridge, New York: Cambridge Univ.Press, 1997.

Gallart, C., Zoccali, M., Aparicio, A., Ann. Rev. Astron. Astrophys. 43, 387 (2005).

Dolphin, A., New Astron. 2, 397 (1997).

Dolphin, A., MNRAS 313, 281 (2000).

Dolphin, A., MNRAS 332, 91 (2002).

Dohm-Palmer, R.C., Skillman, E.D., Saha, A. et al., Astron. J. 114, 2527 (1997).

Dray, L. M., MNRAS 370, 2079 (2006).

Grimm, H.-J., Gilfanov, M., Sunyaev, R., MNRAS 339, 793 (2003).

Girardi, L., Bertelli, G., Bressan, A. et al., Astron. Astrophys. 391, 195 (2002).

Zaritsky, D., Harris, J., Thompson, I.B. et al., Astron. J. 123, 855 (2002).

Zaritsky, D., Harris, J., Thompson, I.B. et al., Astron. J. 128, 1606 (2004).

Illarionov, A. F., Sunyaev, R. A., Astron. Astrophys. 39, 185 (1975).

Kaaret, P., Alonso-Herrero, A., Gallagher, J.S. et al., MNRAS 348, 28 (2004).

Kobulnicky, H., Fryer, C., Kiminki, D., astro-ph/0605069.

Langer, N., Maeder, A., Astron. Astrophys 295, 685 (1995).

Lucy, L.B., Astron. J. 79, 745 (1974).

Lucy, L.B., Astron. Astrophys. 289, 983 (1994).

Massey, P., Astrophys. J. Suppl. Ser. 141, 81 (2002).

Massey, P., Ann. Rev. Astron. Astrophys. 41, 15 (2003).

Maeder, A., Grebel, E. K., Mermilliod, J.-C., Astron. Astrophys., 346, 459 (1999)

Popov, S.B., Prokhorov, M.E., Helmholtz International Summer School and Workshop on Hot points in Astrophysics and Cosmology (astro-ph/0411792) (2004).

Popov, S.B., Lipunov, V.M., Prokhorov, M.E. et al., Astron. Rep. 42, 1, 29 (1998).

Pagel, B.E.J., Tautvaisiene, G., MNRAS 299, 535 (1998).

Russell, S.C., Dopita, M.A., Astrophys. J. 384, 508 (1992).

Udalski, A., Szymanski, M., Kubiak, M. et al., Acta Astron. 48, 147 (1998).

Harris, J., Zaritsky, D., Astron. J. 127, 1531 (2004).

Holtzman, J.A., Gallagher, J.S. III, Cole, A.A. et al., Astron. J. 118, 2262 (1999).

Charbonnel, C., Meynet, G., Maeder, A. et al., Astron. Astrophys. Suppl. Ser. 101, 415 (1993).

Shtykovskiy, P., Gilfanov, M., Astron. Astrophys. 431, 597 (2005).

Shtykovskiy, P., Gilfanov, M., MNRAS 362, 879 (2005).

Schaller, G., Schaerer, D., Meynet, G. et al., Astron. Astrophys. Suppl. Ser. 96, 269 (1992).